Comparative Study on Damage Mechanism of Sandwich Structures with Different Core Materials under Lightning Strikes

Jiangyan Yan [1], Guozheng Wang [2], Qingmin Li[1,*], Li Zhang [2], Joseph D. Yan [3], Chun Chen [4], Zhiyang Fang [4]

[1] State Key Lab of Alternate Electrical Power System with Renewable Energy Sources, North China Electric Power University, Beijing 102206; yanjiangyan@ncepu.edu.cn
[2] School of Electrical Engineering, Shandong University, Jinan 250061
[3] Department of Electrical engineering and Electronics, the University of Liverpool, Liverpool L69 3GJ, UK
[4] Sinoma Wind Power Blade Co. Ltd, Beijing 102100, China

Correspondence: lqmeee@ncepu.edu.cn; Tel.: +86 10 61772040

Abstract: Wind turbine blades are easy to get lightning strikes, which is calling more and more attention in recent years. On such a subject a large current experiment was conducted on 3 typical blade sandwich structures to simulate the natural lightning induced arc effects. Damage condition of different composite materials has been compared: PVC and PET suffered pyrolysis and crack inside, while damage type of balsa wood was fiber breaking off and large lamination between it and resin layer, only a little chemical pyrolysis. To analyze the damage mechanism on sandwich structure with different materials, a FEM (Finite Element Method) model to calculate temperature and pressure distribution was built, and it took into consideration heat transfer and flow expansion due to impulse current. According to simulation results, PVC had most severe temperature and pressure distribution, while PET and balsa wood were in the better condition after experiments. The temperature distribution results explained clearly why balsa wood suffered much less chemical pyrolysis than PVC. Since balsa wood had better thermal stability than PET, pyrolysis area of PET was obviously larger than balsa wood too. Increasing volume fraction of solid components of porous materials can efficiently decrease heat transfer velocity in porous materials. Permeability didn't influence that much. The findings provide supports in materials selecting and designing of blade manufacturing.

Keywords: Wind turbine blade; Lightning strikes; Materials damage; Finite element method (FEM); Temperature distribution; Airflow pressure

1. Introduction

Wind energy expoitation is getting a rapid development for its renewable and environment-friendly characteristics. However, lightning strikes on wind turbine especially on its blades have become an urgent problem as wind turbine becomes higher [1-4]. Blade repairing is very costly because of disassembling and transporting, and it influences the continuity of power supply too.

Wind turbine blade is a composite structure made of laminates with sandwich configurations made from individual sub components joined together with adhesives. A real blade is shown in Figure 1 (a), and the cross-section of the blade is shown in Figure 1 (b). It can be seen in Figure 1 (b) that, the blade consists of two coverings (upper and lower covering stuck together) and two webs inside to hold up the blade structure. The green parts are the main beam and the back trailing edge made of very thick glass fiber to guarantee blade strength. The green-yellow parts are porous

sandwich structures, with polyvinyl chloride (PVC), polyethylene terephthalate (PET) or balsa wood fused to reduce the weight of the whole blade, and usually two layers of glass fiber outside. There are two webs inside the chamber to hold up the too.

(a)

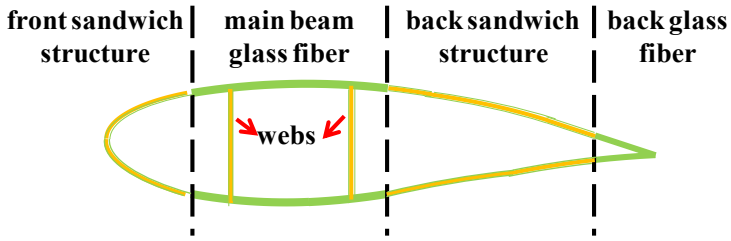

(b)

Figure 1 Blade structure: (a) real blade (b) cross-section of blade

When receptors on blade fail to intercept lightning downward leader, blade materials could get breakdown as lightning induced arc goes through the sandwich structure. Then blade materials would be burnt up, leading to pull apart layers and even the whole blade breaking off [5-9]. A lot of research on lightning attachment position has been done by experimental and numerical methods recently [10-11]. In [12], high voltage experiment was conducted to study possible breakdown position, and results showed that breakdown points were located mostly at sandwich areas. So performance of sandwich structure under thermal effect of lightning induced arc is of great importance from an angle of selection of blade material.

Large current experiment was introduced and laid down in IEC 61400 24(2010) standard to verify the performance of metal receptors under thermal impact of natural lighting [13], and current experiments used to study damage characteristics of wind turbine blade were also reported in [14-20]. Especially, in [21], performance of PVC and balsa wood under lightning current was studied by large current experiment, and its damage mechanism was explained in an angle of chemical pyrolysis via molecular dynamics simulation. However, study on damage characteristic of whole sandwich structure hasn't been reported yet. Actually, materials damage under large current is mainly attributed to the thermal impact and airflow pressure inside porous materials of PVC, PET and balsa wood, so it is essential to study the temperature and pressure distribution inside the sandwich structure. Numerical calculation is effective way to study the instantaneous impact which is really difficult using experimental method. Finite element method (FEM) simulation of thermal and electrical field under lightning strikes has been proposed by different researchers [22-24], but heat transfer and air flow pressure inside porous materials need to be included too to study the whole damage process of sandwich structure.

This paper deals with damage characteristics of sandwich structure with different core materials using large current experiments, and a FEM model was built to calculate temperature and pressure distribution. Based on the above results, damage characteristics for different materials were studied

experimentally and comparatively. The findings provide important advice on blade materials selection in manufacturing process.

2. Large current experiments

2.1. Experimental methods

Blade was simplified into an F-structure (simplified model of blade covering and two webs to hold up the covering in experiments) as shown in Figure 2, and the covering was made of resin and porous materials (PVC, PET and balsa wood) by vacuum casting method. The overall size of all samples is 80cm× 99cm, the heights of each part are 10cm, 42cm, 35cm, and 12cm respectively (up to down). In the sandwich structure, 0.6cm thick PVC, PET and balsa wood were parceled in the middle, with 2 layers of 0.9 mm thick glass fiber reinforced epoxy resin wrapped outside. The materials parameters are shown in Table 1. For porous materials PVC, PET and balsa wood, thermal conductivity, specific heat at constant pressure and density in the table show volume averaging values considering air component. Balsa wood has different thermal conductivities in different orientation because of its anisotropic characteristics (significantly larger along fiber direction, in table 1 the extreme values). The samples were drilled by holes and a 0.01 cm diameter nickel chrome wire was passed through each hole to conduct large current in the different positions shown as red points in Fig.2 (d) (bigger size and number mean larger current values). Pulse current generator is shown in Figure 3. Capacitor voltage (u) was charged to 7.5 kV、 15 kV、30 kV respectively to generate large pulse currents with parameters (intensity and duration) of 6.28 kA (peak value of current)、7.7 (time to peak)/18.1 (half peak time) μs, 12.56 kA、6.7/15.5 μs and 21 kA、5.1/13.1 μs. According to $W=1/2Cu^2$ (C=15.96 μF, is value of charging capacitor), current energy can be obtained as 798 J、1795.5 J and 3192 J. Then damage characteristics were comparatively studied.

(a) (b) (c) (d)

Figure 2 Experimental samples: (a) PVC (b) PET (c) balsa wood (d) nickel chrome wire position

Table 1. Materials parameters

materials	type	thermal conductivity, k, W/(m ·K)	specific heat, C, J/(kg ·K)	density, ϱ, kg/m3	glass transition degree, Tg, K	solid fraction θ(%)
epoxy resin	SWANCOR 2511-1A/1BS	0.4749	989.58	1200	363	100
PVC	3A C70.55	0.0331	1003	66	355	8
PET	3A T92.100	0.0399	1166	98	340	13
Balsa wood	3A SB100	0.0803/0.0661	1047	92	543	11

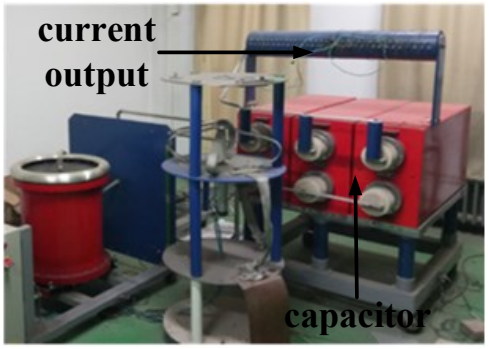

Figure 3 Pulse current generator

2.2. Results and discussion

All the samples got damaged in different degrees as shown in Figure 4. To see inside condition clearly, damaged parts were cut down and pulled apart as shown in Figure 5. PVC and PET sandwich samples got different damage types with respect to balsa wood. They were burnt getting black color near the metal wire, and a large area in lighter color as shown in Figure 4 indicated lamination between resin and porous materials because of airflow expansion damage. While balsa wood was not burnt severely because of its higher pyrolysis temperature, its fiber broke off near metal wire and a large scale of lamination between the interface of balsa wood and resin can be seen in Figure 4 (C). Chemical damage (cd, chemical pyrolysis of core materials which features as black color in Figure 4 and Figure 5) and mechanical damage (md, materials disappearance in light color area shown in Figure 5 and lamination area between resin and core materials shown in Figure 4) sizes were measured in all cases (approximately circular) as shown in Table 2. It reflects that PVC and PET had similar chemical damage radius, but cd of balsa was very small. It is because balsa wood has higher thermal stability (glass transition temperature) than PVC and PET. In the aspect of md, balsa wood had biggest lamination size between resin and balsa wood. Mechanical damage of PVC, PET and balsa wood under pulse current is mainly caused by high temperature and airflow expansion inside, which are hard to be measured in experiments. Then FEM simulation study on the damage characteristic of sandwich structure was done to calculate temperature and pressure distribution quantitatively.

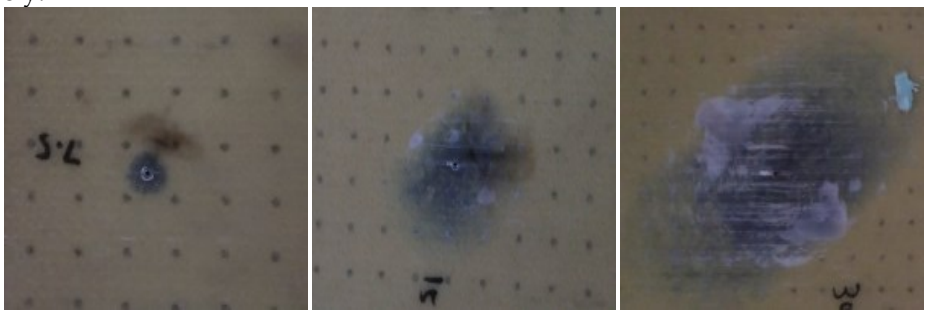

(a)

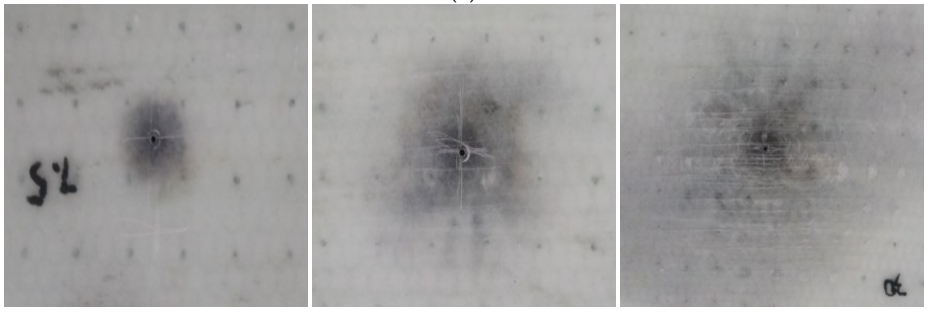

(b)

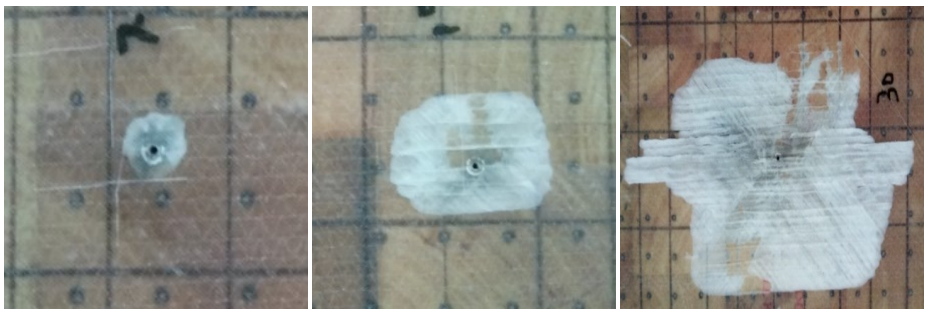

(c)

Figure 4. Damage morphology of samples: (a) PVC (b) PET (c) balsa wood

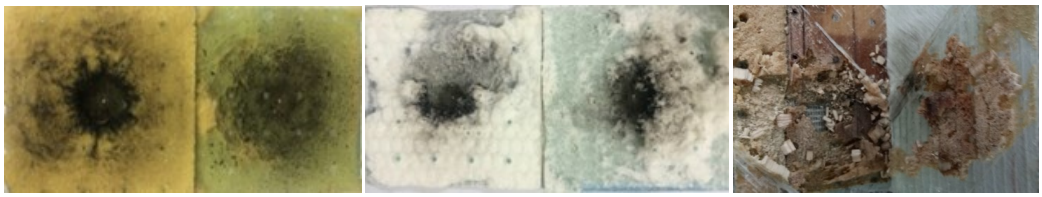

(a) (b) (c)

Figure 5. Inside damage of samples: (a) PVC (b) PET (c) balsa wood

Table 2. Damage radius (cm)

Current peak value (kA)	6.28		12.56		21	
	cd	md	cd	md	cd	md
PVC	0.11	0.50	0.35	3.5	1.7	6.10
PET	0.07	0.45	0.21	3.0	1.5	5.50
Balsa wood	0.01	0.75	0.09	4.1	0.39	7.50

3. Numerical study on the temperature and pressure distribution

FEM model in COMSOL 5.2a was built to calculate temperature and pressure distribution in sandwich structures [25].

3.1. Simulation model

3.1.1. Geometry model

As can be seen from the experimental results, damage is distributed in circular areas, so experimental samples to be simulated by FEM model were simplified into a 2-D axysymmetric model with a proper radius, which is shown in Figure 6.

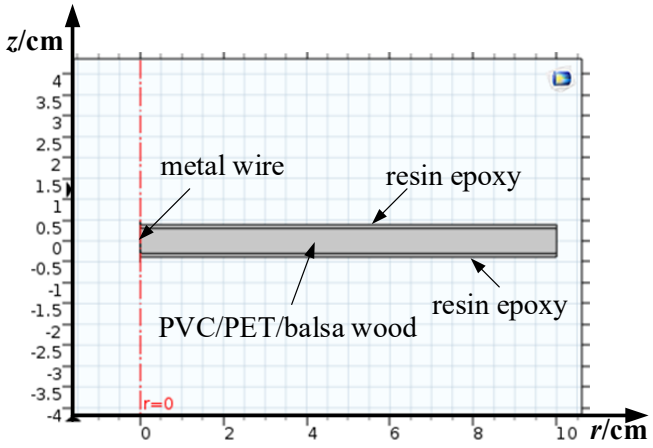

Figure 6. 2-D axisymmetric model for FEM simulation

3.1.2. Large current source

Heat source was given as a large current in the FEM model. Current conservation eq. (1) was applied to calculate the current density, by which resistive heat can be obtained as heat source by eq. (2). Scalar electric potential is provided as the dependent variable as (3).

$$\mathbf{J} = (\sigma + \varepsilon_0 \varepsilon_r \frac{\partial}{\partial t})\mathbf{E} \quad (1)$$

$$Q = \frac{J^2}{\sigma} \quad (2)$$

$$\mathbf{E} = -\nabla V \quad (3)$$

J, current density; σ, conductivity of nickel-chrome wire; ξ_0 , permittivity of vacuum; ξ_r , relative permittivity of nickel-chrome wire; E, electrical field intensity; V, electric potential which was applied on the top of nickel-chrome wire, and it was simplified to be a linear piecewise function, (see eq.(4)) where *A*=6.28 kA, 12.56 kA and 21 kA, are peak values of pulse current and R=0.78Ω is the resistance of nickel chrome wire.

$$V = \begin{cases} RA \times 10^5 t & t < 10^{-6} \\ R(-A \times 10^5 t + 2A) & 10^{-5}\ \text{s} < t < 20^{-6}\ \text{s} \end{cases} \quad (4)$$

3.1.3. Heat transfer in solids, porous materials

First law of thermodynamics, commonly referred to as the principle of conservation of energy was used to calculate heat transfer in different areas.

For the nickel-chrome wire and resin parts, the equation for heat transfer in solids was applied as eq. (5).

$$\rho C \frac{\partial T}{\partial t} - \nabla \cdot (k \nabla T) = Q \quad (5)$$

T, temperature; *t*, time; ρ, density; *C*, heat capacity; *k*, thermal conductivity; *Q*, heat source.

The first term on the left is energy increasing of the whole system, the second term is heat flux by conduction from neighbor elements because of temperature gradient.

PVC, PET and balsa wood are porous materials, and they have a similar expression of conservation of energy as shown in eq. (6). Comparing eq.(6) with eq.(5) for solid material, $\rho_g C_g \mathbf{u} \cdot \nabla T$ was added to describe the heat flux by gas convection from neighbor elements. Since there is gas fraction in porous materials, heat transfer by gas convection should be included too.

Heat capacity and thermal conductivity of porous materials were calculated by volume averaging of gas and solid components, as shown in eq. (7) and eq. (8).

$$\rho C \frac{\partial T}{\partial t} + \rho_g C_g \mathbf{u} \cdot \nabla T - \nabla \cdot (k \nabla T) = Q \tag{6}$$

$$\rho C = \theta \rho_g C_g + (1-\theta) \rho_s C_s \tag{7}$$

$$k = \theta k_g + (1-\theta) k_s \tag{8}$$

u, velocity field; ρ_s, solid density; C_s, solid heat capacity; k_s, solid thermal conductivity; ρ_g, air density, it changes with temperature T and pressure P, that is $\rho_g = \frac{P \mathrm{M}_g}{\mathrm{R}T}$. M_g=28.97 g/mol, is air molar mass and R=8.314J/（mol · K）, is gas constant; C_g, gas heat capacity; k_g, gas thermal conductivity; ρ, C and k are density of porous matrix; θ is porosity.

To simulate practical condition, all outer boundaries were set as eq. (9) considering the convection process between samples and external atmosphere.

$$-\mathbf{n} \cdot \mathbf{q} = h(T_{ext} - T) \tag{9}$$

n is normal vector; q is heat flux on the boundaries; h=15 W/(m^2 ·K) is heat transfer coefficient on materials' surface; T_{ext} is atmosphere temperature.

3.1.4. Fluid dynamics in porous materials

Brinkman equations was adopted to calculate the fluid dynamics in porous materials. The flow in porous media is governed by a combination of the continuity eq. (10) and the momentum conservation eq. (11), which together form the Brinkman equations. Pressure P and velocity vector **u** are independent variables.

$$\frac{\partial}{\partial t}(\theta \rho_g) + \nabla \cdot (\rho_g \mathbf{u}) = Q_{br} \tag{10}$$

$$\frac{\rho_g}{\varepsilon}\left(\frac{\partial \mathbf{u}}{\partial t} + (\mathbf{u} \cdot \nabla)\frac{\mathbf{u}}{\varepsilon}\right) = -\nabla P + \nabla \cdot \left\{\frac{1}{\varepsilon}\left[\mu(\nabla \mathbf{u} + (\nabla \mathbf{u})^T) - \frac{2}{3}\mu(\nabla \cdot \mathbf{u})\mathbf{I}\right]\right\} - \left(\boldsymbol{\kappa}^{-1}\mu + \frac{Q_{br}}{\varepsilon^2}\right)\mathbf{u} + \mathbf{F} \tag{11}$$

μ, dynamic viscosity of air in porous materials; **u**, velocity vector; p, pressure; $\boldsymbol{\kappa}$=1×10^{-13}m^2, permeability tensor of the porous medium; Q_{br}=0, mass source or mass sink; **F**, force term, influence of gravity and other volume forces, and it was neglected in this model.

To simulate the real condition, the right boundary was set as outlet boundary, and **u**=0 for other boundaries to baffle expansion flow.

3.1.5. Multi-Physics coupling

The above discussed calculation procedure involving a coupled threefold physics, as is shown in Figure 7, allowed to obtain temperature T and pressure P. A damage process lasting 1000μs was simulated

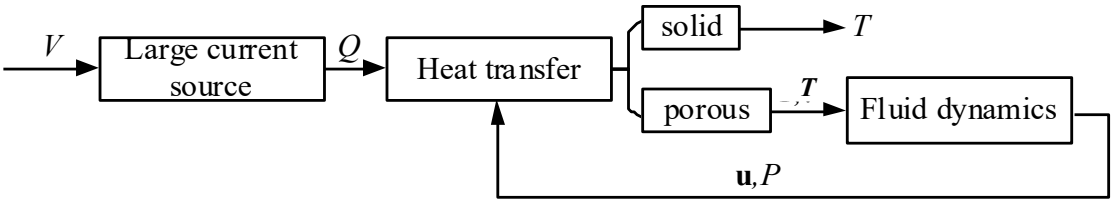

Figure 7 Multi-physics coupling

3.2. Simulation results

3.2.1. Temperature distribution

Temperature distributions after calculations inside sandwich materials are shown in Figure 8. It can be seen that heat is transferred much quicker in porous materials than in resin. It is because that airflow convection promoted heat transfer inside porous material, especially under the very big fluid velocity under impulse energy of thousands of degree. Resin layer conducted heat slowly and most heat released to the atmosphere, so there was no serious damage in this area.

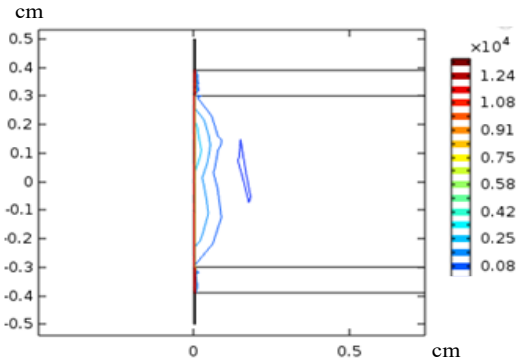

(a)

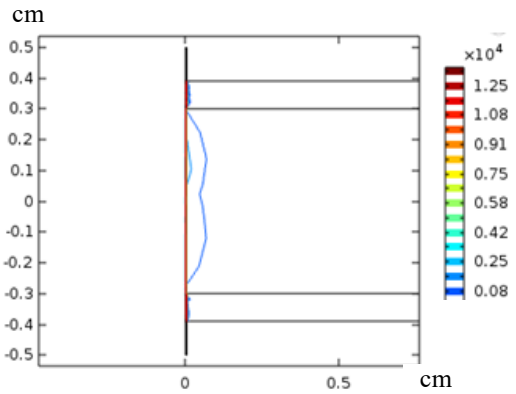

(b)

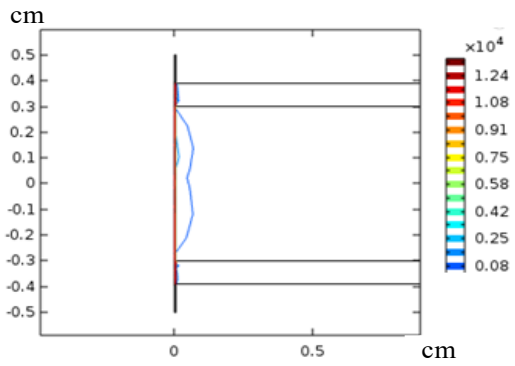

(c)

Figure 8. Isothermal curve in sandwich models (peak value of 12.56kA, 50μs): (a) PVC (b) PET (c) balsa wood

PVC porous materials had smallest solid fraction, that is, highest air fraction, so its high temperature scale was obviously larger than others. Simulation areas with temperature above glass transition temperature were considered as chemical damage areas, which turned black in practice. Then chemical damage radius of different materials was estimated with respect to time as is shown in Figure 9. The last data connected by dotted lines is experimental results in Table 2. It can be seen that the trend of simulation data fitted well with experimental results. Chemical damage radius increased quickly when current peak value was raised. Balsa wood had smallest chemical damage radius among three materials. It is because of its highest glass transition temperature. PVC had largest radius because of its higher temperature distribution.

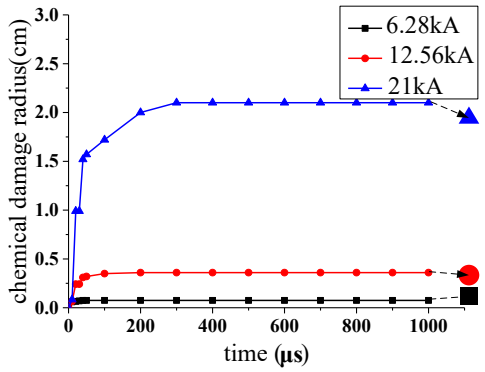

(a)

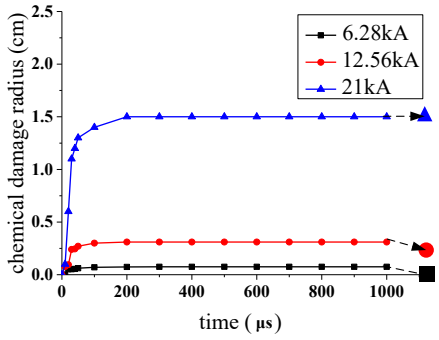

(b)

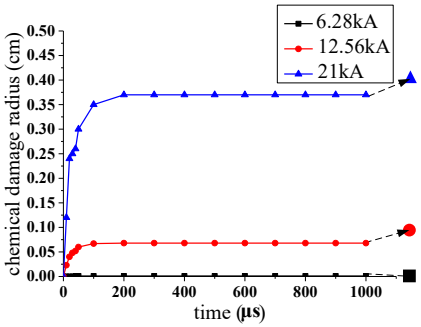

(c)

Figure 9. Chemical damage radius of porous materials: (a) PVC (b) PET (c) balsa wood

3.2.2 Pressure distribution

Porous materials also suffered severe physical damage from inner flow pressure. Pressure distribution at 200μs is shown in Figure 10. Consistent with temperature distribution, PVC is intended to suffer much more severe fluid impact pressure than PET and balsa wood because of high temperature and large air fraction. Peak value of pressure in different points on center line in r-direction is shown in Figure 11. In the aspect of balsa wood, it performs better inside, but when high pressure occurred at its interface with resin, large lamination happened because of weak bonding between wood and resin.

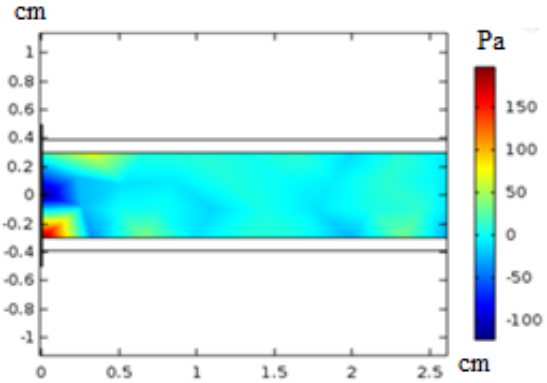

(a)

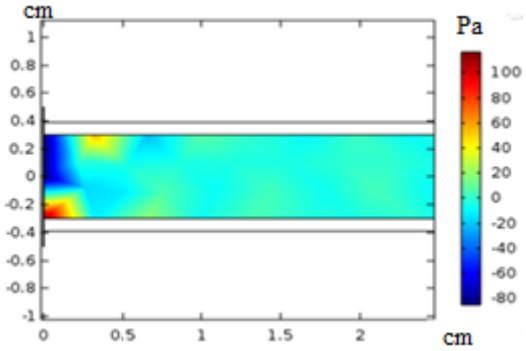

(b)

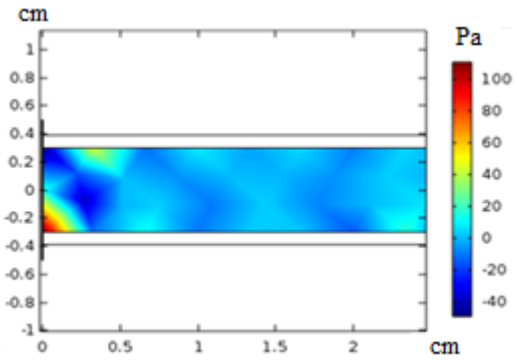

(c)

Figure 10. Pressure distribution in porous areas (peak value of 6.28kA, 200μs): (a) PVC (b) PET (c) balsa wood

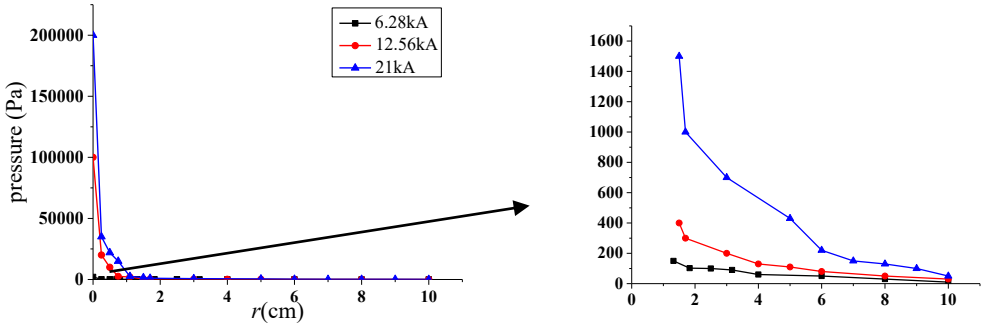

(a)

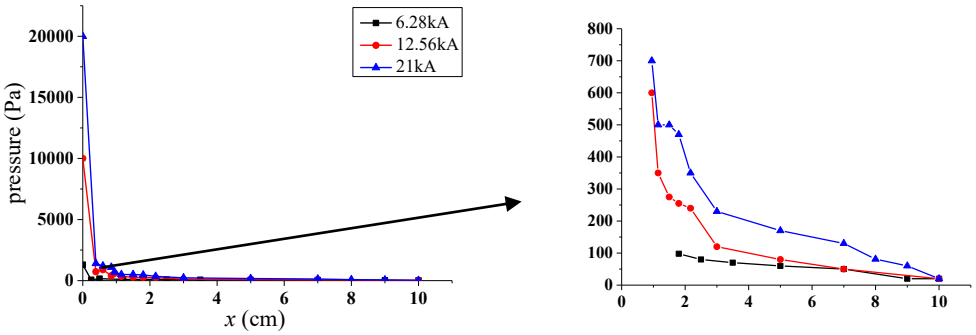

(b)

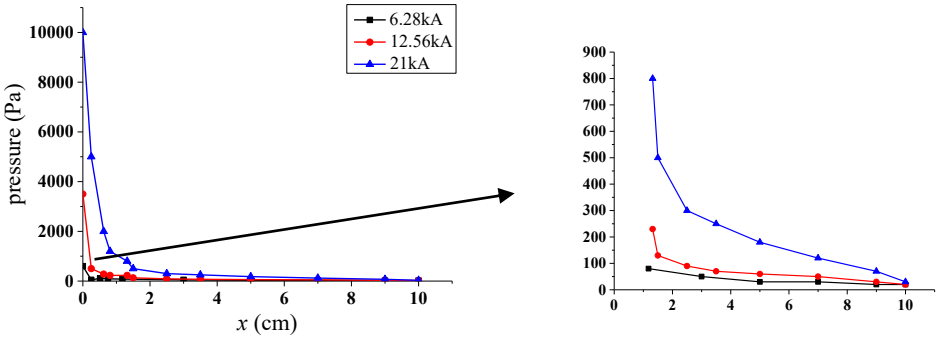

(c)

Figure 11. Pressure distribution on center line of porous materials: (a) PVC (b) PET (c) balsa wood

3.2.2 Influence of porosity, permeability

Solid materials' volume fraction (θ) and permeability are main parameters for porous materials in heat transfer and fluid dynamics process. Based on the above model, roles of porosity and permeability were analyzed which helped materials designing for wind turbine blade. Since permeability hardly influenced the thermal conducting and airflow expansion process because of very small dynamic viscosity of air (see eq. (11)), only results for different porosities will be presented.

Glass transition scale and area radius where $P > 100$Pa were set as standards for thermal and fluid dynamics results. θ of real value as shown in Table 1, 2 times of real value, 3 times of real value and 5 times of real value were used to compare their influence, as shown in Table 3 and Table 4. It is indicated that increasing solid fraction obviously decreases the damage area. It can be explained in this way: when large current goes through porous materials, the heat transfers through 3 ways: heat conduction by solid fraction, heat convection by gas fraction and going out by current channels to outside environment. Compared to heat conduction by solid fraction (PVC, PET and balsa wood are not so good at conducting heat), heat convection by gas fraction and gonging out play more important role in heat transfer because airflow has very large velocity. Heat convection by gas fraction accelerates heat to be transferred to larger scale of porous materials to cause more severe damage. So if the gas fraction of porous materials is decreased, that is, solid fraction is increased, the damaged area can be decreased, and more energy goes out by current channels to outside environment.

Table 3. Glass transition scale reduction (%) with θ

Solid fraction	1 time	2 times	3 times	5 times
PVC	0	22.5	68.7	72.6
PET	0	17.7	70	73.3
Balsa wood	0	30.7	49.3	86.7

Table 4. Pressure (> 100Pa) area radius reduction (%) with porosities

Solid fraction	1 time	2 times	3 times	5 times
PVC	0	2.6	5.1	23.1
PET	0	3.6	22.1	26.3
Balsa wood	0	3.2	20.6	25.9

4. Conclusions

Large current experiments to compare damage characteristics of sandwich structure with different core materials were conducted in this experimental study, and FEM simulation was used to reveal the damage mechanism. Combining experiments and simulation results, it can be concluded what follows:

1. PVC, PET and balsa wood all got severe damage under large current, but their damage types were different: PVC and PET suffered serious pyrolysis and crack inside, while damage of balsa wood sample was fiber breaking off and large lamination at its interface with resin layer. Balsa wood was burnt only in a little part under experimental current.

2. Porous materials transferred heat much faster than resin layer, because fast air-flow convection under the thermal impact from lightning promoted strongly heat transfer in porous materials layer.

3. PVC sample had highest average value of temperature and pressure because of highest air fraction and airflow convection, so it suffered the biggest mechanical damage and chemical damage; and balsa wood had relatively less chemical damage because of higher glass transition temperature. Balsa wood is very soft, which makes it good at reducing expansion pressure inside, while bad bonding between it and resin layer resulted in large lamination at the interface with resin. However, when energy of lightning current is extremely large, balsa wood usually catches fire more likely than

PVC and PET because of its own characteristics, and in worst condition, its fire lasts for a long time to cause serious fire hazard.

4. If the gas fraction of porous materials is decreased, that is, solid fraction is increased, heat transfer by gas convection in porous materials can be decreased. Then the damaged area can be reduced and more energy goes out by current channels to outside environment in practice. It is a good way to reduce damage scale of porous materials under lightning strikes.

Acknowledgments: This work was supported by the National Natural Science Foundation of China (grant numbers 51420105011, 51677110).

Author Contributions: Jiangyan Yan conceived and designed the experiments; Qingmin Li, Li Zhang and Joseph D. Yan gave important advice on the experiments; Chun Chen and Zhiyang Fang contributed experimental materials; Jiangyan Yan and Guozheng Wang performed the experiments; Jiangyan Yan performed the simulation, analyzed the data and finally wrote the paper.

References

1. Candela Garolera A.; Find Madsen S.; Nissim M. Lightning Damage to Wind Turbine Blades from Wind Farms in the U.S, *IEEE transactions on power delivery*, 2016, 31(3): 1043-1049.
2. Napolitano F.; Paolone M.; Borghetti A.. Models of Wind-Turbine Main-Shaft Bearings for the Development of Specific Lightning Protection Systems, *IEEE transaction on electromagnetic compatibility*, 2011, 53(1): 99-107.
3. Rodrigues B.; Mendes F.; Catalão S. Protection of Wind Energy Systems Against the Indirect Effects of Lightning, *Renewable energy*, 2011, 36(2011): 2888-2996.
4. Li X.; Wang J.; Wang Y.. Lightning Transient Characteristics of Cable Power Collection System in Wind Power Plants, *IET renewable power generation,* 2015, 9(8): 1025–1032.
5. Candela Garolera A.. Lightning Protection of Flap System for Wind Turbine Blades, *Ph.D. thesis,* Technical University of Denmark, Denmark, 2014.
6. Yokoyama S.; Yasuda Y.; Minowa M.; Sekioka S.. Clarification of The Mechanism of Wind Turbine Blade Damage Taking Lightning Characteristics into Consideration and Relevant Research Project, *International conference on lightning protection (ICLP)*, Vienna, Austria, 2012.
7. Yasuda Y.; Yokoyama S.; Idenno M.. Verification of Lightning Damage Classification to Wind Turbine Blades. *International conference on lightning protection (ICLP)*, Vienna, Austria, 2012.
8. Arinaga S.; Tsutsumi K.. Experimental Study on Lightning Protection Methods for Wind Turbine Blades, *International conference on lightning protection*, Kanazawa, Japan, 2006.
9. Yokoyama S. Lightning Protection of Wind Turbine Blades, *Electric power systems research*, 2013, 94(2013): 3-9.
10. Zhou M.; Wang J.; Fan Y. Experimental Study of Lightning Strike Attachment Characteristics on Wind Turbine Generators, *International conference on lightning protection (ICLP),* Estoril, Portugal, 2017.
11. Long M.. On the Attachment of Lightning Flashes to Wind Turbines, *Ph.D. thesis,* KTH Royal Institute of Technology, Sweden, 2016.
12. YanJ.; Li Q.; Guo Z. Puncture Position on Wind Turbine Blades and Arc Path Evolution under Lightning Strikes, *Materials and Design*, 2017, 122 (2017) 197–205.
13. IEC 61400-24: 2010: Wind turbines -Part 24: Lightning protection, 2010.
14. Rachidi F.. A Review of Current Issues in Lightning Protection of New Generation Wind-turbine Blades, *IEEE transactions on industrial electronics*, 2008, 55(2008): 2489-2496.
15. Yokoyama S.. Lightning Protection of Wind Turbine Blades, *Electric power systems research,* 2013, 94(2013): 3-9.
16. Radicevi M.; Savic S.; Madsen F.; Badea I.. Impact of Wind Turbine Blade Rotation on the Lightning Strike Incidence -A Theoretical and Experimental Study Using a Reduced-size Model, *Energy*, 2012, 25(2012) 644-654.
17. Inoue K.; Korematsu Y.; Nakamura N.. Study on Damage-mechanism of Wind Turbine Blades by Lightning Strike, *International conference on lightning protection*, Kanazawa, Japan, 2006.
18. Goda Y.; Tanaka S.; Ohtaka T.. Arc Tests of Wind Turbine Blades Simulating High Energy Lightning Strike, *International conference on lightning protection*, Uppsala, Sweden, 2008.

19. Ogasawara T.; Hirano Y.; Yoshimura A.. Coupled Thermal–electrical Analysis for Carbon Fiber epoxy Composites Exposed, *Composites: Part A*, 2010, 41(2010): 973-981.
20. Feraboli P.; Miller M.. Damage Resistance and Tolerance of Carbon/epoxy Composite Coupons Subjected to Simulated Lightning Strike, *Composites: Part A: Applied Science and Manufacturing*, 2009, 40(6): 954–967.
21. Yan J.; Li Q.; Guo Z.. Damage Mechanism of PVC and Balsa Wood Used in Wind Turbine Blade under Thermal Effect of Lightning Strikes, *International Conference on Lightning Protection (ICLP)*, Estoril, Portugal, 2017.
22. WangY.; Zhupanska I.. Lightning Strike Thermal Damage Model for Glass Fiber Reinforced Polymer Matrix Composites and Its Application to Wind Turbine Blades, *Composite Structures*, 2015, 132 (2015) 1182–1191.
23. Ding N.; Zhao B.; Liu Z.. Simulation of Ablation Damage of Composite Laminates Subjected to Lightning Strikes, *Acta aeronautica et astronautica sinica*, 2013, 34(2): 301-308.(in Chinese)
24. Ding N,; Zhao B.. Analysis of Damage Influence Factors on Ablation Damage of Composite Laminates Subjected to Lightning Strikes, *Transactions of materials and heat treatment*, 2014, 35(2): 186-192. (in Chinese)
25. Yu C.. Numerical analysis of heat and mass transfer for porous materials, *Tsinghua University press*, 2011.